

TR-o-0045

98

Modelling of Slot Coupled, Circular Microstrip Patch
Antenna Elements

Claus Baumer

1992. 4. 17.

ATR光電波通信研究所

Modelling of Slot Coupled, Circular Microstrip Patch Antenna Elements

Claus Baumer

ATR

Optical and Radio Communications Research Laboratories

Soraku-gun, Kyoto 619-02, Japan

Content of ATR Technical Report

1992/4/13

1. **Name:** Claus Baumer
2. **Laboratory:** Optical and Radio Communications Research Laboratories
3. **Theme:** Modelling of slot coupled, circular microstrip patch antenna elements
4. **Period:** December 1990 – April 1992
5. **Affiliation:** University of Stuttgart, Institut für Hochfrequenztechnik,
Pfaffenwaldring 47, D 7000 Stuttgart 80, Federal Republic of Germany
6. **Description of Research:** See chapter 1 of the report, in which an introduction to the research topic is given and in which the motivation to conduct this research is explained.
7. **Other:**
8. **Summary:** An analysis method for slot coupled, circular microstrip patch antenna elements is described. The method is well suited for CAD applications due to its low computational requirements. The report contains a detailed description of the theoretical background. Calculated results are compared with measurements.
9. **Publications:**
 - C.Baumer *Analysis of slot coupled, circular microstrip patch antennas using cavity method.* IEICE Technical Report, 1991, Vol. 91, No. 214, pages 13–19; presented at the Technical IEICE Meeting in Sapporo, Japan.
 - C.Baumer *Modelling of slot coupled, circular microstrip patch antennas.* 1992, Proceedings of the 1992 IEICE Spring Conference, page 2 – 85, Noda, Japan.
 - C.Baumer *Analysis of slot coupled, circular microstrip patch antennas.* 1992, to be submitted to Electronics Letters.

Insight, not numbers!

unknown

Contents

Preface	4
1 Introduction	5
2 Theoretical Background	9
2.1 Simple Cavity Model	11
2.2 Use of the Cavity Model in an Aperture Coupled Configuration	12
2.2.1 Green's function approach	13
2.2.2 Expansion of Fields	14
2.2.3 Eigenvectors of a Circular Cylindrical Cavity	17
2.3 The Input Admittance of a Cavity	19
2.3.1 Solution Using the Eigenvector Approach	19
2.3.2 Solution Using a Green's Function Approach	19
2.3.3 Losses	20
2.4 Aperture Field	20
2.5 Feeding Structure	21
2.6 Complete Structure	21
2.7 Parasitic models	23
2.7.1 Fringing fields	24
2.7.2 Open stub and feeding line	24
2.7.3 Surface waves	24
3 Examples	26
3.1 Green's function approach	26
3.2 Eigenvector approach	31
4 Summary	38

A	Remarks concerning measurements	40
B	Some useful equations	42
	Bibliography	45

Preface

The work described in this report has been done at ATR Optical and Radio Communications Laboratories during my stay as a visiting researcher from December 1990 to April 1992. The research topic is related to the development of an active phased array antenna for mobile communications at Ka- or Ku-frequency band.

An analysis method for slot coupled, circular microstrip patch antenna elements is proposed. The method is well suited for CAD applications due to its low computational requirements. Chapter 1 contains a brief introduction. A detailed description of the theory developed is given in chapter 2. In Chapter 3 various results are discussed. The comparison of measurements and calculated results gives an impression of the efficiency of the method derived.

The author would like to thank Dr.Y.Furuhama, President of ATR Optical and Radio Communications Research Laboratory and Dr.M.Fujise, Head of Radio Communications Department, who provided the opportunity and the encouragement to carry out this work. I am also grateful to the members of the antenna group for their valuable suggestions and their constructive criticisms.

Chapter 1

Introduction

In the last few years, the concept of active phased array antennas in microstrip technology has attracted considerable attention. In this type of microstrip antenna, phase shifters and amplifiers are integrated on a semiconductor substrate along with the feed network and the radiating elements. The basic set up of such an antenna is shown in figure 1.1. It consists of two substrate layers, which are separated by a conducting ground plane. The radiating elements are connected to the active circuitry via apertures in the conducting ground plane in this example.

Other possibilities to connect microstrip patches to a feeding structure or an active device have been proposed and four major feeding techniques together with their advantages and drawbacks are shown in figure 1.2. However, we will limit our discussion to aperture coupled devices (see figure 1.3), since it seems to be one of the most promising feeding methods for future active array antennas.

Since the concept of using aperture-coupling for feeding microstrip antennas was introduced by Pozar [20], a number of theoretical and experimental investigations have been reported, which obtain input impedance or radiation pattern of such structures. For a full wave analysis in space- or spectral domain, mostly the Method of Moments has been applied [21],[27],[23]. Although these approaches seem to deliver quite accurate results for input impedance or radiation pattern, they usually require a large amount of computation time. This holds as well for time domain methods like Transmission Line Method or Spatial Network Method [13].

To avoid a full wave analysis, the "cavity model" has widely been used in the analysis of coaxial fed patch antennas. The solutions obtained for that case, cannot easily be applied to the aperture coupling type of feeding, which is being investigated in this report.

Only a few papers describe the application of the cavity model together with slot coupling

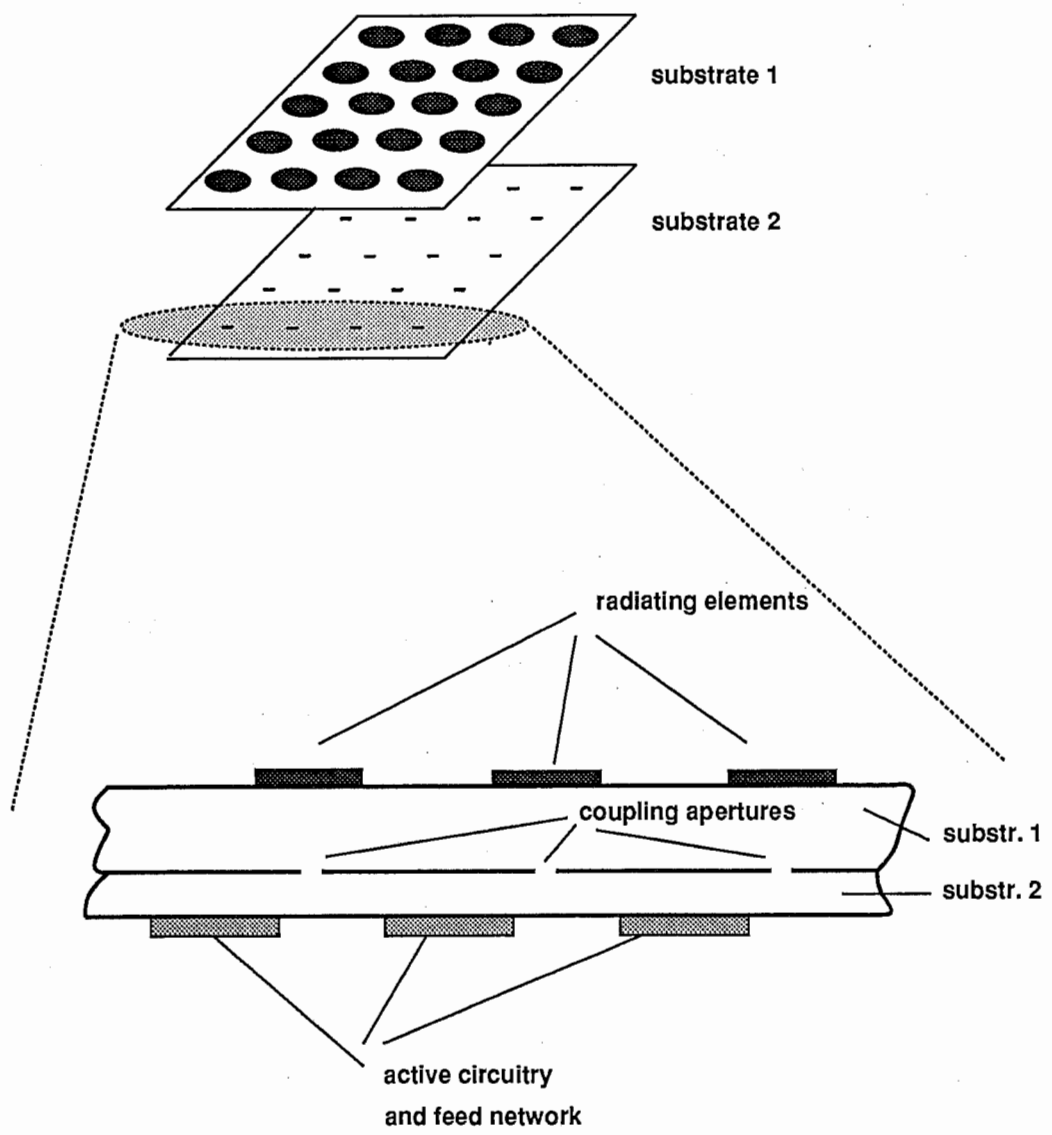
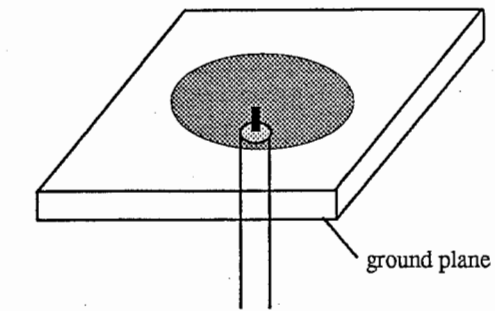
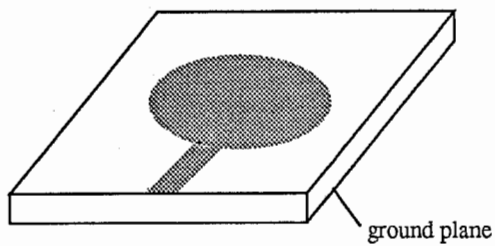


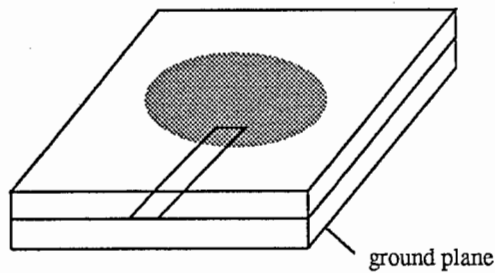
Figure 1.1: Configuration of an active array antenna



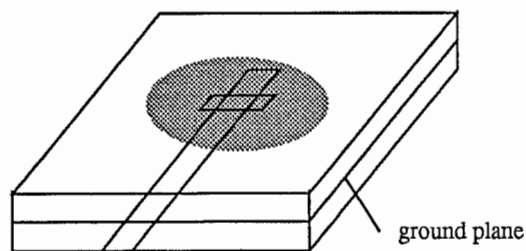
- + no feed line radiation loss
- + different value of Z obtainable by adjusting feed location
- + Z of patch on thin substrate can easily be obtained
- complicated and costly in fabrication



- + possible to manufacture antenna and feeding line in one step
- antenna and feeding line are on same substrate side, resulting in erratic radiation at high frequencies



- + flexible design
- two layers of substrate required



- + very flexible design
- + different values of Z obtainable by adjusting aperture shape and location

Figure 1.2: Basic methods for exciting the TM_{11} -mode in a circular microstrip patch antenna (+ = advantages, - = disadvantages, Z = input impedance)

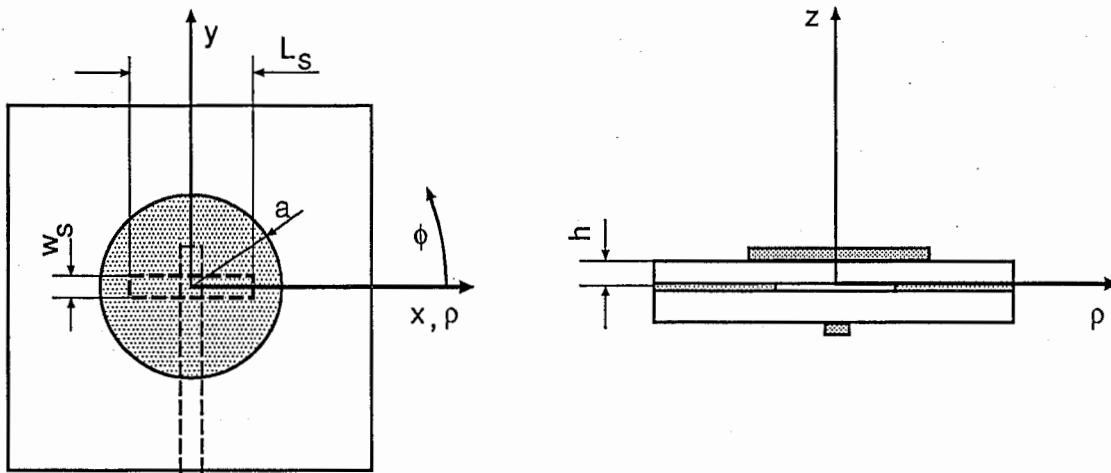


Figure 1.3: Geometry of aperture coupled, circular patch (top view and cross section)

for rectangular patches [1], [11], [14]. In [1] an analysis is described, which uses a Green's function approach in which the slot is modelled through a uniform magnetic current source throughout the substrate thickness. The paper does not discuss the interconnection between patch element and feed line. In [11] the slot effect is described by the equations for the fields in the cavity and a slot line. This slot line needs additional analysis [10]. The analysis suggested in [14] seems to be valid for small slots only, since the volume integral over the slot volume in the application of the Poynting theorem was neglected. Two ways of analysing circular, slot coupled patches will be described in this report. The first one is an extension of the analysis reported in [1]. The second one uses a different approach, with which the shortcomings of [1], [11], [14] can be avoided. The aperture coupling problem is formulated in a way close to Moment Method Solutions. The solution described can be seen as a "one-term" moment solution, since the impedances involved are scalars and not matrices.

Chapter 2

Theoretical Background

The general problem of aperture coupling has to be solved. Since the literature on this problem is extensive, only two books for further reading shall be recommended here. These are [9] and [7], which give comprehensive introductions and references to other literature.

The problem of coupling between two regions will be treated in such a way that the law of conservation of flux at the aperture is applied [9] (fig. 2.1)

$$\oint_{apert} (\mathbf{E}_{tan}^a \times \mathbf{H} ds)_{region1} = \oint_{apert} (\mathbf{E}_{tan}^a \times \mathbf{H} ds)_{region2}. \quad (2.1)$$

After assuming the tangential electric field \mathbf{E}_{tan} in the aperture, region 1 and region 2 can be considered separately. The original problem has thus been divided into two parts. After separately analysing each of them, the two parts can be combined by applying the continuity equation given above.

Applying this idea to a slot coupled patch element (fig.1.3) gives the following two parts:

- The first part is a dielectrically filled, circular cavity, which is formed through the volume under the patch and which is loaded with a rectangular slot.
- The second part is a microstrip line on an infinite dielectric slab with a slot in the ground plane.

These two parts (fig. 2.2) are then linked together by conserving the flux of reaction at the aperture plane according to eqn.(2.1).

The theoretical background which is necessary to apply this method to slot coupled patch element antennas is described in the subsequent sections.

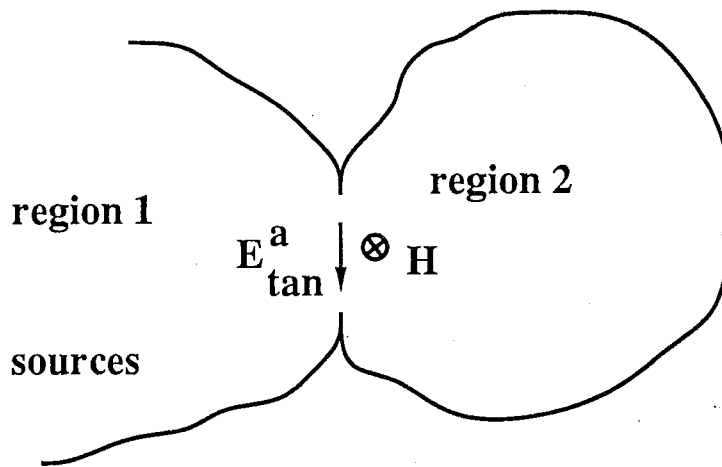


Figure 2.1: General aperture problem

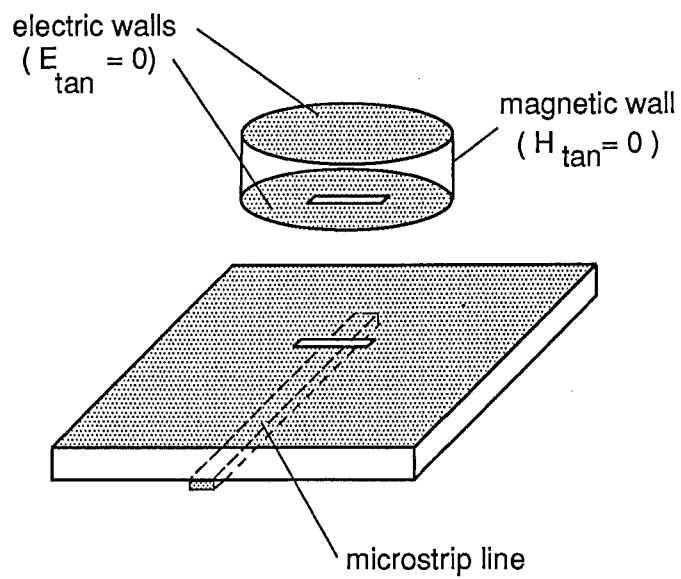


Figure 2.2: Basic model of the slot coupled patch element

2.1 Simple Cavity Model

Microstrip patch antennas belong to the class of planar circuits, which have two dimensions comparable to the wavelength and a third dimension (substrate height h) much smaller than the wavelength λ . If $h \ll \lambda$, the first assumption of the cavity model is, that the electrical field \mathbf{E} under the patch is independent of the z -coordinate (a coordinate system as shown in fig. 2.2 is used) and has only a z -component, namely

$$\mathbf{E} = \hat{z}E_z(r, \rho) \quad (2.2)$$

and second, that the patch perimeter can be enclosed by magnetic walls. Thus the field inside the dielectric region of the microstrip can be determined by solving a cavity problem, where the cavity is formed by the volume under the patch. In a simple cavity model, no sources are considered and the wave equation can be written as

$$(\nabla^2 + k^2)E_z = 0 \quad (2.3)$$

where $k = \omega\sqrt{\mu\epsilon}$. The fields inside the cavity must satisfy this equation and the magnetic wall boundary condition, which is

$$\frac{\partial E_z}{\partial \rho} = 0 \quad \text{for} \quad \rho = a \quad (2.4)$$

Thus for a circular cavity (radius a) a solution of eqn.(2.3) is

$$E_z = E_0 J_m(k_m \rho) \cos(m\phi) \quad (2.5)$$

where $J_m(k_m \rho)$ are Bessel functions of order m . The derivative of E_z must vanish at $\rho = a$. Hence we must have

$$J'_m(k_m a) = 0 \quad (2.6)$$

from which the eigenvalues may be determined. The above equation can be satisfied by choosing

$$k_m = \frac{x'_{mn}}{a} \quad (2.7)$$

where x'_{mn} is the n 'th zero of the derivative of the Bessel function of order m . Using this in equation (2.5) gives

$$E_z = E_0 J_m\left(\frac{x'_{mn}\rho}{a}\right) \cos(m\phi). \quad (2.8)$$

The resonant frequency f_{mn} of the mn -mode in the cavity can be given as

$$f_{mn} = \frac{x'_{mn}c}{2\pi a\sqrt{\epsilon_r}} \quad (2.9)$$

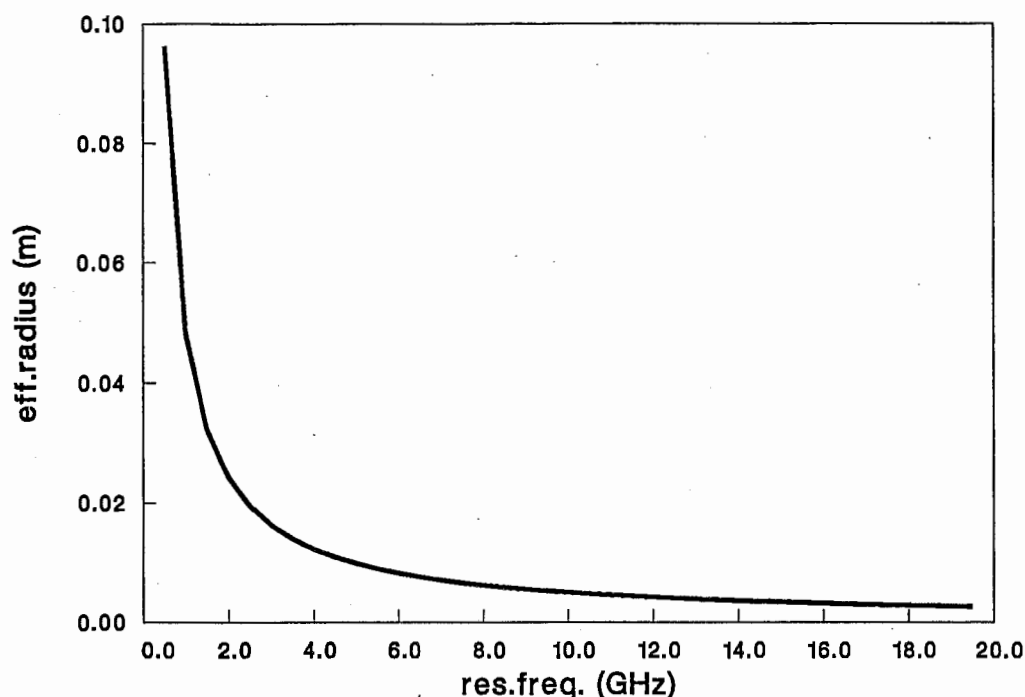


Figure 2.3: Effective patch radius vs. resonant frequency (substrate height = 0.75mm, rel. permittivity = 3.37)

where c is the velocity of light in free space and ϵ_r the relative permittivity of the substrate material.

To give an example, the effective patch radius as a function of resonant frequency is calculated using equations (2.68), (2.9) and is plotted in figure 2.3 for a substrate with relative permittivity $\epsilon_r = 3.37$ and a substrate height $h = 0.75\text{mm}$. Note the considerable decrease in patch size for frequencies in the Ku-Band region (12GHz – 18GHz) compared to the L-Band frequency region (1GHz – 2GHz).

2.2 Use of the Cavity Model in an Aperture Coupled Configuration

No sources are included in the simple cavity model as described in section 2.1. The problem one has to consider in the case of aperture coupled patches, is how to characterize

the electromagnetic field adequately in a dielectrically filled, simply connected, doubly bounded cavity, which is excited via an aperture in the bottom wall.

Two methods will be described. The first one is a Green's function approach, whereas the second method uses an expansion of fields in irrotational and solenoidal eigenvectors.

2.2.1 Green's function approach

In this section, a Green's function approach is described, with which the magnetic field in the slot loaded cavity can be obtained. For a cavity in which magnetic and electric current sources exist, Maxwell's equations are

$$\nabla \times \mathbf{E} = -j\omega\mu\mathbf{H} - \mathbf{J}_{mag} \quad (2.10)$$

$$\nabla \times \mathbf{H} = j\omega\epsilon\mathbf{E} + \mathbf{J}_{el} \quad (2.11)$$

where

\mathbf{E} = electric field

\mathbf{H} = magnetic field

\mathbf{J}_{mag} = magnetic current source

\mathbf{J}_{el} = electric current source

If there are only magnetic current sources in the cavity, the wave equation in \mathbf{E} can be given as

$$\nabla^2\mathbf{E} + \omega^2\mu\epsilon\mathbf{E} = \nabla \times \mathbf{J}_{mag} \quad (2.12)$$

Since the electrical field shall only have a z-component, the appropriate equation for the Green's function (G) is

$$\nabla^2 G_z + \omega^2\mu\epsilon G_z = \delta(x - x')\delta(y - y') \quad (2.13)$$

The primed coordinates (x', y') indicate the area occupied by the source, over which the integration has to be performed afterwards. The unprimed coordinates represent the observation point.

The Green's function can be obtained by expanding it in terms of known eigenfunctions ψ_m of the corresponding Helmholtz equation, satisfying

$$\nabla^2\psi_m + \omega^2\mu\epsilon\psi_m = 0 \quad (2.14)$$

with the boundary condition

$$\frac{\partial \psi_m}{\partial n} = 0 \quad \text{at } r = a. \quad (2.15)$$

The vector \mathbf{n} is a unit normal and directed outwards. The solution of the above equations can easily be obtained

$$\psi_m = \psi_0 J_m\left(\frac{x'_{mn}\rho}{a}\right) \cos(m\phi) \quad (2.16)$$

The Green's function can then be given as

$$G_z(x, y, x', y') = \sum_{m,n=0}^{\infty} \frac{\psi_{mn}(x', y') \psi_{mn}(x, y)}{k^2 - k_{mn}^2} \quad (2.17)$$

An integration over the area of the source has to be performed to obtain the electric field E_z in the cavity

$$E_z(x, y) = \oint G_z(x, y; x', y') [\nabla' \times \mathbf{M}(x', y')]_z dx' dy' \quad (2.18)$$

The magnetic field \mathbf{H} can then be obtained from

$$\mathbf{H} = -\frac{\nabla \times \mathbf{E}}{j\omega\mu} - \frac{\mathbf{J}_{mag}}{j\omega\mu} \quad (2.19)$$

Only a brief description of the theory related to Green's functions can be given here. More comprehensive descriptions may be found in [3],[13].

2.2.2 Expansion of Fields

The most general electromagnetic field in a cavity can be obtained as a superposition of an infinite number of elementary solutions (normal modes) [7] [9].

Helmholtz's theorem states, that a general vector field \mathbf{P} can be splitted in a solenoidal part ($\nabla \cdot \mathbf{P} = 0$) and a lamellar part ($\nabla \times \mathbf{P} = 0$). Consequently two sets of orthogonal functions are used, one set solenoidal, the other irrotational. The solenoidal set respectively the irrotational set is used to expand the solenoidal part respectively the irrotational part of the field. Both, the electric field and the magnetic field will be expanded in its own set.

The electric field in the cavity will be expanded in terms of solenoidal modes \mathbf{E}_m and irrotational modes \mathbf{F}_m and the magnetic field in the cavity will be written in terms of solenoidal modes \mathbf{H}_m and irrotational modes \mathbf{G}_m .

In case of a patch antenna element, two different types of boundaries exist. One is the electric boundary S given by the top (patch) and bottom (ground plane) of the circular

cavity, the other one is the magnetic boundary S' given by the side walls of the cavity. The field expansion for this case, where mixed boundary conditions have to be imposed, is explained in the following.

The solenoidal electric modes \mathbf{E}_m are solutions of

$$(\nabla^2 + k_m^2)\mathbf{E}_m = 0 \quad (2.20)$$

$$\mathbf{n} \times \mathbf{E}_m = 0 \quad \text{and} \quad \nabla \cdot \mathbf{E}_m = 0 \quad \text{on } S \quad (2.21)$$

$$\mathbf{n} \times \nabla \times \mathbf{E}_m = 0 \quad \text{and} \quad \mathbf{n} \cdot \mathbf{E}_m = 0 \quad \text{on } S' \quad (2.22)$$

and for the \mathbf{F}_m

$$\mathbf{F}_m = \frac{1}{l_m} \nabla \Phi_m \quad (2.23)$$

where

$k_m, l_m =$ eigenvalues

$\Phi_m =$ scalar functions.

The Φ_m are solutions of

$$(\nabla^2 + l_m^2)\Phi_m = 0 \quad (2.24)$$

with

$$\Phi_m = 0 \quad \text{on } S \quad \text{and} \quad \frac{\partial \Phi_m}{\partial n} = 0 \quad \text{on } S' \quad (2.25)$$

Similarly, the equations for the solenoidal magnetic modes \mathbf{H}_m are

$$(\nabla^2 + k_m^2)\mathbf{H}_m = 0 \quad (2.26)$$

with

$$\mathbf{n} \times \nabla \times \mathbf{H}_m = 0 \quad \text{and} \quad \mathbf{n} \cdot \mathbf{H}_m = 0 \quad \text{on } S \quad (2.27)$$

$$\mathbf{n} \times \mathbf{H}_m = 0 \quad \text{and} \quad \nabla \cdot \mathbf{H}_m = 0 \quad \text{on } S' \quad (2.28)$$

and for the \mathbf{G}_m

$$\mathbf{G}_m = \frac{1}{p_m} \nabla \Psi_m \quad (2.29)$$

where

$p_m =$ eigenvalue

$\Psi_m =$ scalar functions.

The Ψ_m are solutions of

$$(\nabla^2 + p_m^2)\Psi_m = 0 \quad (2.30)$$

with

$$\Psi_m = 0 \quad \text{on } S' \quad \text{and} \quad \frac{\partial \Psi_m}{\partial n} = 0 \quad \text{on } S \quad (2.31)$$

To ensure the equality of the normalization integrals, the \mathbf{E}_m and \mathbf{H}_m shall satisfy the relations

$$k_m \mathbf{E}_m = \nabla \times \mathbf{H}_m \quad \text{and} \quad k_m \mathbf{H}_m = \nabla \times \mathbf{E}_m. \quad (2.32)$$

The normalization integrals are

$$\epsilon \int_V \mathbf{E}_i \cdot \mathbf{E}_j dV = \begin{cases} 0 & \text{if } i \neq j \\ 1 & \text{if } i = j \end{cases} \quad (2.33)$$

$$\mu \int_V \mathbf{H}_i \cdot \mathbf{H}_j dV = \begin{cases} 0 & \text{if } i \neq j \\ 1 & \text{if } i = j \end{cases} \quad (2.34)$$

$$\epsilon \int_V \mathbf{F}_i \cdot \mathbf{F}_j dV = \begin{cases} 0 & \text{if } i \neq j \\ 1 & \text{if } i = j \end{cases} \quad (2.35)$$

$$\mu \int_V \mathbf{G}_i \cdot \mathbf{G}_j dV = \begin{cases} 0 & \text{if } i \neq j \\ 1 & \text{if } i = j \end{cases} \quad (2.36)$$

For a more detailed description of the expansion of fields in solenoidal and irrotational eigenvectors see [26],[7].

The expansions of the electric and magnetic fields in a circular cylindrical cavity can then be given as follows

$$\mathbf{E} = \sum e_m \mathbf{E}_m + f_m \mathbf{F}_m \quad (2.37)$$

$$\mathbf{H} = \sum h_m \mathbf{H}_m + g_m \mathbf{G}_m \quad (2.38)$$

where e_m, f_m, h_m, g_m are amplitude constants. These constants can be derived in the usual way. Eqns.(2.37),(2.38) have to be inserted into Maxwell's equations and the orthogonality relations have to be applied. The amplitude constants are derived to be

$$e_m = \frac{-j\omega\mu\epsilon \int \mathbf{J}_{el} \cdot \mathbf{E}_m dV - k_m\epsilon \int \mathbf{H}_m \cdot \mathbf{J}_{mag} dV + k_m\epsilon \oint \mathbf{H}_m \times \mathbf{E} ds}{k_m^2 - \omega^2\mu\epsilon} \quad (2.39)$$

$$f_m = \frac{-1}{j\omega} \int_V \mathbf{J}_{el} \cdot \mathbf{F}_m dV \quad (2.40)$$

$$h_m = \frac{-j\omega\mu\epsilon \int_V \mathbf{H}_m \cdot \mathbf{J}_{mag} dV + j\omega\mu\epsilon \oint \mathbf{H}_m \times \mathbf{E} ds + k_m\mu \int_V \mathbf{J}_{el} \cdot \mathbf{E}_m dV}{k_m^2 - \omega^2\mu\epsilon} \quad (2.41)$$

$$g_m = \frac{1}{j\omega} \left[\oint \mathbf{G}_m \times \mathbf{E} ds - \int_V \mathbf{G}_m \cdot \mathbf{J}_{mag} dV \right] \quad (2.42)$$

The electric and magnetic fields due to a slot in the bottom wall of a circular cavity of height h and of radius a with magnetic sidewalls and electric walls on top and bottom, free of electric or magnetic volume sources can then be determined.

$$\mathbf{E} = \sum_m \frac{k_m \epsilon \oint \mathbf{H}_m \times \mathbf{E}_{tan}^a ds}{(k_m^2 - k^2)} \mathbf{E}_m \quad (2.43)$$

$$\mathbf{H} = \sum_m \left[\frac{j\omega\mu\epsilon \oint \mathbf{H}_m \times \mathbf{E}_{tan}^a ds}{(k_m^2 - k^2)} \right] \mathbf{H}_m + \frac{1}{j\omega} \sum_m \oint \mathbf{G}_m \times \mathbf{E}_{tan}^a ds \cdot \mathbf{G}_m \quad (2.44)$$

where

$\mathbf{H}_m, \mathbf{E}_m =$ solenoidal eigenvectors of the cavity

$\mathbf{G}_m =$ irrotational magnetic eigenvectors

$\mathbf{E}_{tan}^a =$ tangential electric field in the aperture

$k_m =$ eigenvalue

$k =$ wavenumber

$ds =$ surface element directed outward from the cavity volume.

The integration has to be performed over the slot aperture. Eqns. (2.43), (2.44) are the formal solution of the cavity problem. The fields are uniquely determined by knowledge of the tangential electric field in the coupling aperture.

It can be seen from eqns.(2.43), (2.44) that the terms in \mathbf{E}_m and \mathbf{H}_m have a coefficient of the form $N/(k_m^2 - k^2)$. This describes a resonant behaviour. It is to be noted, that no resonance phenomenon exists for the terms in \mathbf{G}_m .

2.2.3 Eigenvectors of a Circular Cylindrical Cavity

With the assumption $\partial/\partial z = 0$ and the appropriate boundary conditions, the solenoidal magnetic eigenvectors in the cavity can be derived to be

$$H_{m,\rho} = \frac{1}{\rho} B_m J_m(k_m \rho) \begin{Bmatrix} -m \sin(m\phi) \\ m \cos(m\phi) \end{Bmatrix} \quad (2.45)$$

$$H_{m,\phi} = -B_m k_m J'_m(k_m \rho) \begin{Bmatrix} \cos(m\phi) \\ \sin(m\phi) \end{Bmatrix} \quad (2.46)$$

$$k_m = x'_{mn}/a \quad (2.47)$$

where

$$' = \frac{\partial}{\partial(k_m \rho)} \quad (2.48)$$

and $m = 0, 1, 2, 3, \dots$ $n = 1, 2, 3, 4, \dots$ The normalization integral is given as

$$\mu \int_V |\mathbf{H}_m|^2 dV = B_m^2 \frac{\pi h \mu}{\epsilon_m} (k_m^2 a^2 - m^2) J_m^2(k_m a) \quad (2.49)$$

J_m = Besselfunction of order m ,

x'_{mn} = n -th zero of the derivative of Besselfunction of order m ,

ϵ_m = Neumanns factor ($\epsilon_m = 1$ for $m = 0$; $\epsilon_m = 2$ for $m = 1, 2, 3, \dots$),

h = heighth of cavity.

The solenoidal electric eigenvectors can be derived to be

$$E_{m,z} = B_m \frac{1}{j\omega\epsilon} k_m^2 J_m(k_m \rho) \begin{Bmatrix} \cos(m\phi) \\ \sin(m\phi) \end{Bmatrix} \quad (2.50)$$

The equations for the irrotational modes G_m are

$$G_{m,\rho} = A_m \begin{Bmatrix} \sin(m\phi) \\ m \cos(m\phi) \end{Bmatrix} J'_m(p_m \rho) \quad (2.51)$$

$$G_{m,\phi} = -A_m \begin{Bmatrix} \cos(m\phi) \\ -\sin(m\phi) \end{Bmatrix} m J_m(p_m \rho) \quad (2.52)$$

$$p_m = \frac{x_{mn}}{a} \quad (2.53)$$

The normalization integral for the irrotational modes is given as

$$\mu \int_V |\mathbf{G}_m|^2 dV = A_m^2 \frac{1}{\epsilon_m} \pi h \mu a^2 J_m'^2(p_m a) \quad (2.54)$$

where

J'_m = derivative of Besselfunction of order m ,

x_{mn} = n -th zero of the Besselfunction of order m ,

ϵ_m = Neumanns factor ($\epsilon_m = 1$ for $m = 0$; $\epsilon_m = 2$ for $m = 1, 2, 3, \dots$),

h = heighth of cavity.

2.3 The Input Admittance of a Cavity

2.3.1 Solution Using the Eigenvector Approach

An aperture admittance definition according to [9] shall be used here

$$\underline{Y}_{apert} = \frac{1}{V_0^2} \oint_{apert} \mathbf{E}_{tan}^a \times \mathbf{H} ds, \quad (2.55)$$

where V_0 is some reference voltage. This is strictly speaking not an admittance, since the conjugate complex of \mathbf{H} is not used. However, we adopt this definition, since this is more convenient. Using the definition and eqns.(2.1),(2.33),(2.44) gives

$$\underline{Y}_{apert} = \frac{1}{V_0^2} \frac{1}{j\omega} \sum_m a_m^2 + \frac{1}{V_0^2} \sum_m \frac{j\omega\epsilon\mu b_m^2}{k_m^2 - \omega^2\mu\epsilon} \quad (2.56)$$

$$a_m = \oint_{apert} \mathbf{E}_{tan}^a \times \mathbf{G}_m ds \quad (2.57)$$

$$b_m = \oint_{apert} \mathbf{E}_{tan}^a \times \mathbf{H}_m ds \quad (2.58)$$

This equation expresses the input impedance at the aperture plane of the cavity and can be interpreted as a network consisting of an inductance in parallel with an infinite number of series resonant circuits. Each series resonant circuit corresponds to a mode of the cavity.

The amplitude of excitation of a mode depends on the value of the amplitude coefficients (a_m, b_m in Equation (2.56)). There is no excitation for example, when \mathbf{E}_{tan}^a is parallel to \mathbf{H}_m or parallel to \mathbf{G}_m .

2.3.2 Solution Using a Green's Function Approach

In [1] a Green's function approach and a magnetic current source formulation has been used to calculate the electric field under the patch. The expression for the magnetic field in the cavity was derived in section 2.2.1.

If the procedure suggested in [1] is used, an expression for the input impedance at the slot aperture can be derived. A sinusoidal field distribution in the aperture was assumed.

$$\underline{Y}_{apert} = \frac{2l_s}{j\omega\mu h w_s} + \sum_m \frac{j\omega\epsilon l_s^2 b_m^2}{h^2 \omega_s^2 (k_m^2 - k^2)} \quad (2.59)$$

2.3.3 Losses

As long as there is no dissipation, the input admittances derived above will be purely reactive and they would become infinite at resonant frequencies.

However, in a real cavity the amplitude of the fields is limited due to the inevitable losses. These losses consist mainly of radiation loss, dielectric loss, conductor loss and surface wave loss. The radiation loss, which is not a loss, but a wanted radiation should contribute most to the quality factor.

In literature there are two suggestions to account for losses. In [9] the resonant frequency is taken to be complex,

$$\omega_i^2 = \omega_r^2(1 + j/Q), \quad (2.60)$$

where Q is the overall quality factor of the patch and is defined as

$$Q = \frac{\omega W}{P} \quad (2.61)$$

W = energy stored

P = average power dissipated

In [22] the wavenumber k of the principal mode is replaced by an effective wavenumber k_{eff}

$$k_{eff} = \sqrt{\epsilon_r(1 - j\delta_{eff})}k \quad (2.62)$$

thus lumping all losses into a single "dielectric loss" with dielectric loss tangent δ_{eff} (see [9] p.50 in addition). The loss tangent is related to the quality factor Q by $\delta_{eff} = 1/Q$. It can be shown, that for a cavity with moderately high Q the exact value of k is not needed for the evaluation of Q . An accurate value of Q can be obtained even though the energy W and the power P are calculated using the wavenumber k instead of k_{eff} [22].

How to obtain the quality factor due to space wave, dielectric losses and metallization losses shall not be discussed here. The reader may refer to [18], [2], [5], where detailed discriptions are given. The effect of surface wave losses is considered in section 2.7 of this report.

2.4 Aperture Field

The field in the coupling aperture has to be assumed in such a way, that the physical field distribution is met to a certain extent. Using a narrow slot as coupling aperture reduces

this problem, since one dimension of the slot is small compared to the wavelength and only a field depending on one coordinate has to be assumed.

The electric field can be expanded in a set of sinusoidal modes. However, it has been shown, that a single mode approximation is actually quite good [21]. Therefore the field in the slot is expressed as

$$\mathbf{E}_{tan}^a = \frac{V \sin(k_a(L_s/2 - |x|))}{w_s \sin(k_a L_s/2)} \mathbf{n}_y \quad \text{for} \quad |x| < \frac{L_s}{2}, \quad |y| < \frac{w_s}{2}. \quad (2.63)$$

V is a reference voltage and k_a is the effective wavenumber in the slot. A good choice for k_a is the average of the two wavenumbers in the two regions adjacent to the slot [21].

2.5 Feeding Structure

For the second part of the analysis, the impedance properties of a slot in the ground plane of a microstrip line have to be characterized.

The modal voltage discontinuity ΔV in the microstrip line due to the slot has to be obtained in a first step. The discontinuity in modal voltage (ΔV) due to the slot is given as

$$\Delta V = \oint_{apert} \mathbf{E}_{tan}^a \times \mathbf{H}_{MS} ds \quad (2.64)$$

where \mathbf{H}_{MS} is the normalized transverse modal vector function for the magnetic field of the dominant mode in the microstrip-line.

The slot admittance \underline{Y}_s can be given as

$$\underline{Y}_s = \frac{\oint_{apert} \mathbf{E}_{tan} \times \mathbf{H} ds}{(\Delta V)^2} \quad (2.65)$$

$\Delta V/V$ as a function of relative slotlength was calculated for a substrate height of $h_{MS} = 1.5\text{mm}$. The relative permittivities of feed line substrate and patch element substrate have been chosen to be $\epsilon_r = 2.55$ (Fig. 2.4). It can be seen, that there is a slot resonance at $l_s/\lambda_0 \approx 0.31$. This value is smaller than $l_s/\lambda_0 = 0.5$ due to the loading with dielectric material.

2.6 Complete Structure

The model which was used to analyse the slot coupled patch element consists of two parts as explained in the beginning of this chapter. It has been shown in [21] that a slot coupled

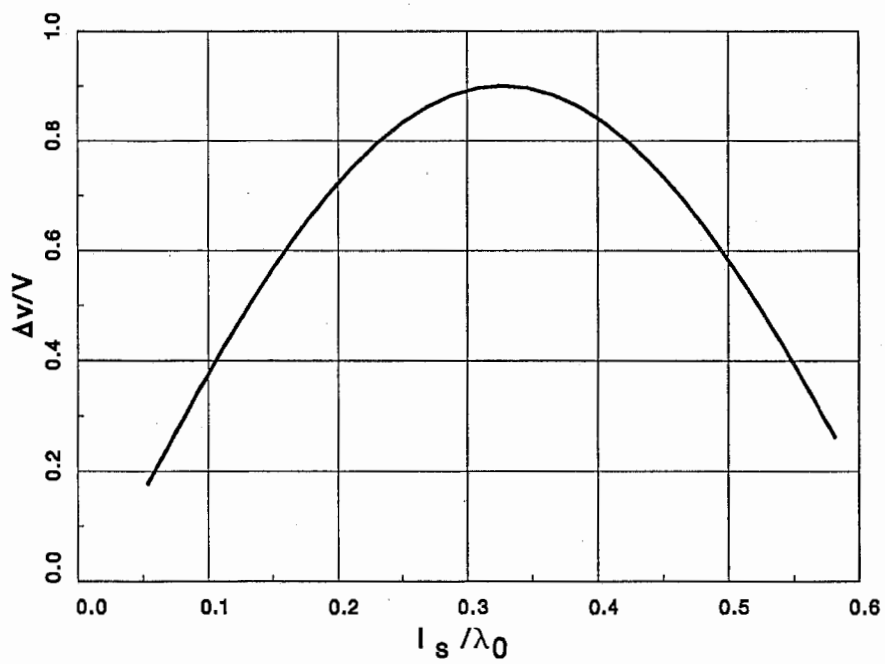


Figure 2.4: Calculated modal voltage discontinuity as a function of relative slotlength ($h_{MS} = 1.5\text{mm}$, $\epsilon_{r,cav} = 2.55$, $\epsilon_{r,ms} = 2.55$)

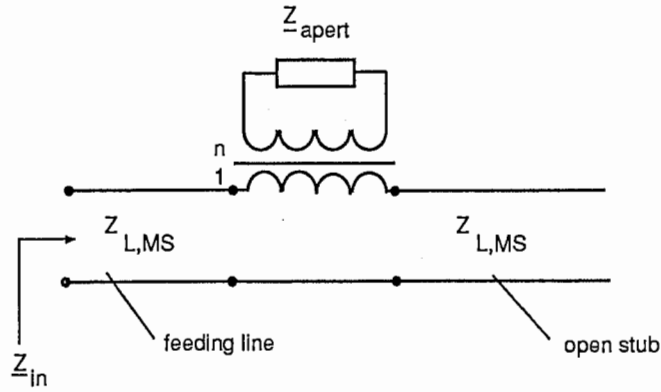


Figure 2.5: Equivalent circuit of an aperture coupled patch element

patch element forms a series discontinuity in the feeding microstrip line. This leads to an equivalent circuit as shown in figure 2.5. The ideal transformer is introduced to account for possible impedance levels in both problems.

To determine the transformation ratio n of the ideal transformer, one has to note that the aperture admittance \underline{Y}_{apert} is defined with respect to a voltage V_0 and that the discontinuity in modal voltage in the feeding line is ΔV ; hence

$$n^2 = \frac{V_0^2}{(\Delta V)^2}. \quad (2.66)$$

The normalized transformed input admittance of the complete structure can be obtained as [21]

$$\underline{y}_{trans} = \frac{n^2 \underline{Y}_{apert} + \underline{Y}_s}{Y_{L,MS}}, \quad (2.67)$$

where $Y_{L,MS}$ is the characteristic impedance of the microstripline and \underline{Y}_s is the external slot impedance as given in eqn.(2.65).

The open stub and other circuitry can now be included in the analysis using suitable models.

2.7 Parasitic models

So far only the basic theory has been described. To improve the accuracy of the calculations and to make this theory applicable for a CAD package, a number of additional physical effects have to be included in the analysis.

2.7.1 Fringing fields

Eqn. (2.9) is based on the assumption of perfect magnetic walls and does not take into account the fringing fields at the edge of the microstrip patch. To account for fringing fields an effective radius a_{eff} , which is slightly larger than the radius a , can be introduced [28],[24],[6]. In the following the formula of [24] is given.

$$a_{eff} = a \left[1 + \frac{2h}{\pi \epsilon_r a} \left\{ \ln \left(\frac{\pi a}{2h} \right) + 1.7726 \right\} \right]^{1/2} \quad (2.68)$$

with

h = height of substrate

a = physical patch radius

ϵ_r = permittivity of substrate material.

2.7.2 Open stub and feeding line

The fringing fields at the end of an open stub are usually compensated through an extension of the line length [12], [8]. A more accurate characterization suitable for high frequencies is given in [16]. The open stub is described through a terminal admittance \underline{Y}

$$\underline{Y} = G_r + G_s + jB. \quad (2.69)$$

The conductances G_r and G_s are due to the radiation loss and the surface wave loss respectively. The susceptance B represents the storage of energy created by the evanescent fields near the termination.

2.7.3 Surface waves

At higher frequencies the possibility of excitation of surface guided waves has to be considered. A basic treatment of the problem is given in [9]. For a grounded dielectric slab the cutoff frequencies for the TM_n and TE_n surface modes are given by

$$f_c = \frac{nc_0}{4h\sqrt{\epsilon_r - 1}} \quad (2.70)$$

where $n = 0, 2, 4, \dots$ for TM-modes and $n = 1, 3, 5 \dots$ for TE-modes. There is no cutoff frequency for the TM_0 mode.

Some estimates on the effect of surface waves can be found in literature: James et. al [17] estimated the surface wave excitation for patch element antennas and found that it is not

important if $h/\lambda_0 < 0.09$ for $\epsilon_r = 2.3$ and $h/\lambda_0 < 0.03$ for $\epsilon_r = 10.0$. Wood [29] gave a more precise estimation: no more than 25% of the total radiated power are launched as a surface wave, if $h/\lambda_0 < 0.07$ for $\epsilon_r = 2.3$ and $h/\lambda_0 < 0.023$ for $\epsilon_r = 10$.

The reader may refer to [5] or [18], for the analytical treatment of surface waves in patch antenna applications. Relative simple expressions for the calculation of the surface wave effect have been given in [19], [15].

Chapter 3

Examples

3.1 Green's function approach

In this section some results are presented, which have been obtained using the Green's function approach, which was described in section 2.3.2.

Figure 3.1 shows the measured and calculated resonant frequencies as a function of slot length for an L-band patch element. The expression "resonant frequency" is used for that frequency, at which the best input impedance match of the patch was obtainable by adjusting the stub length. Measured and calculated values for the real part of the input impedance of the patch element at the resonant frequency are compared in figure 3.2. The experimental results have been taken from [25]. The dimensions for the L-Band patch element are given in table 3.1. An effective radius a_{eff} according to equation (2.68) was chosen, to account for fringing effects at the edge of the circular patch.

Figure 3.3 shows the behaviour of the resonant frequency of a Ku-band patch as a function of slot length for two different patch radii. The lower plot compares measurement and calculation for a patch radius $a = 3.73\text{mm}$ and the upper plot is for a patch radius of

patch	radius	32.63mm	
slot	width	1.5mm	slot length varied
substrate 1	height	3.2mm	rel. permittivity 2.55
substrate 2	height	1.6mm	rel. permittivity 2.55
feeding line	width	4.3mm	stub length adjusted

Table 3.1: Dimensions of the L-band patch element

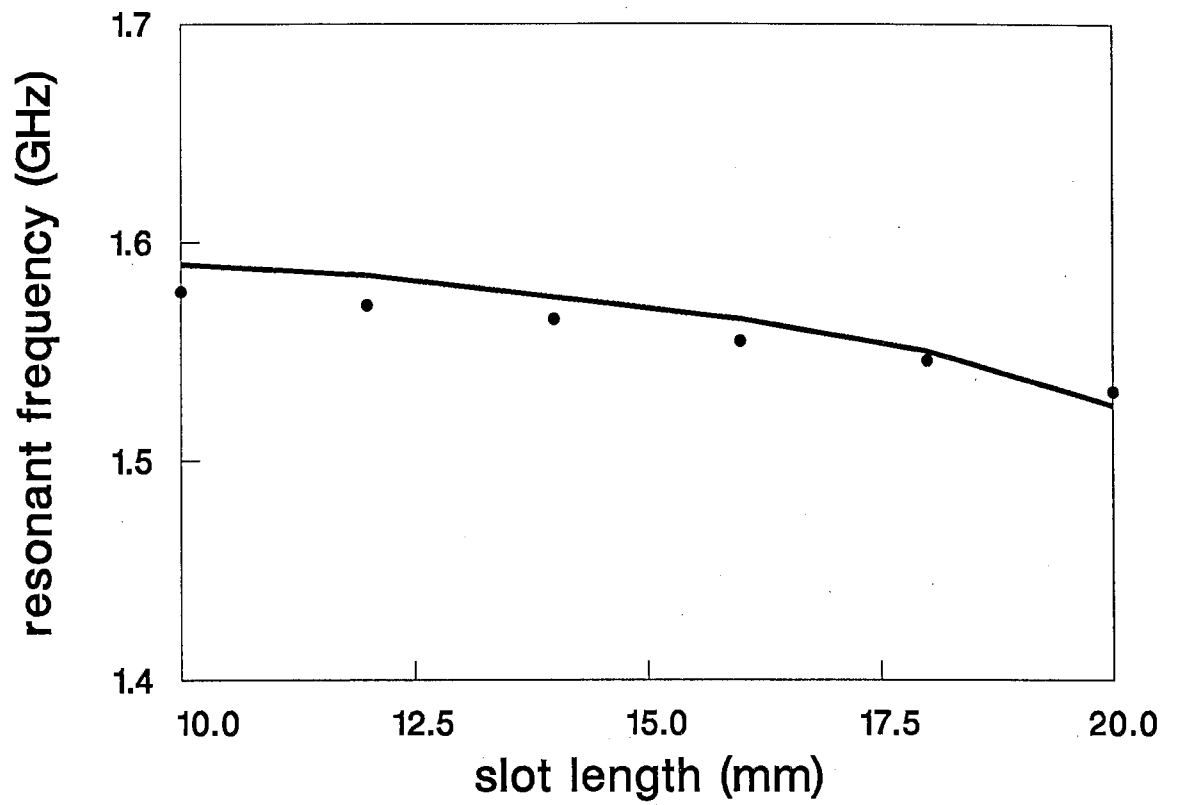


Figure 3.1: Resonant frequency of the L-band patch element versus slot length (calculated: —, measured: • •)

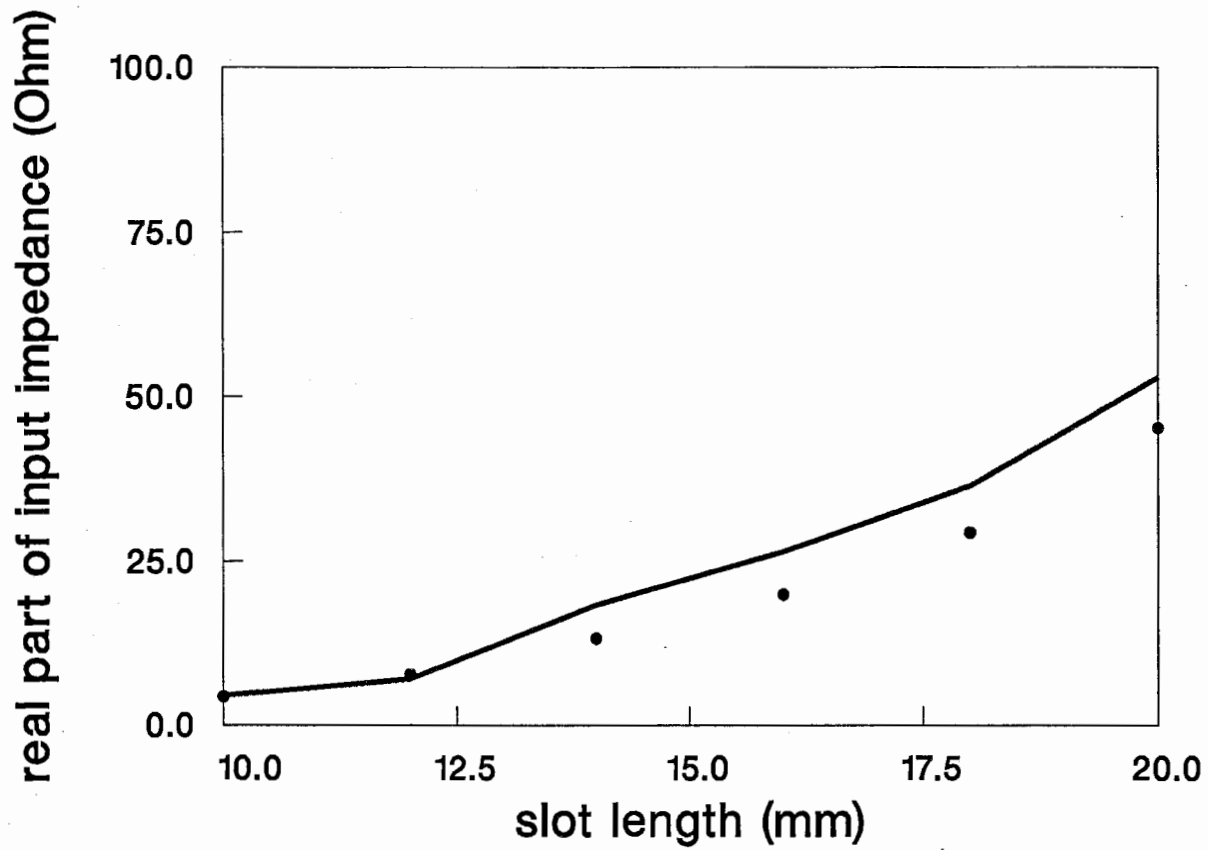


Figure 3.2: Real part of input impedance of the L-band patch versus slot length at resonant frequency (calculated: —, measured: • •)

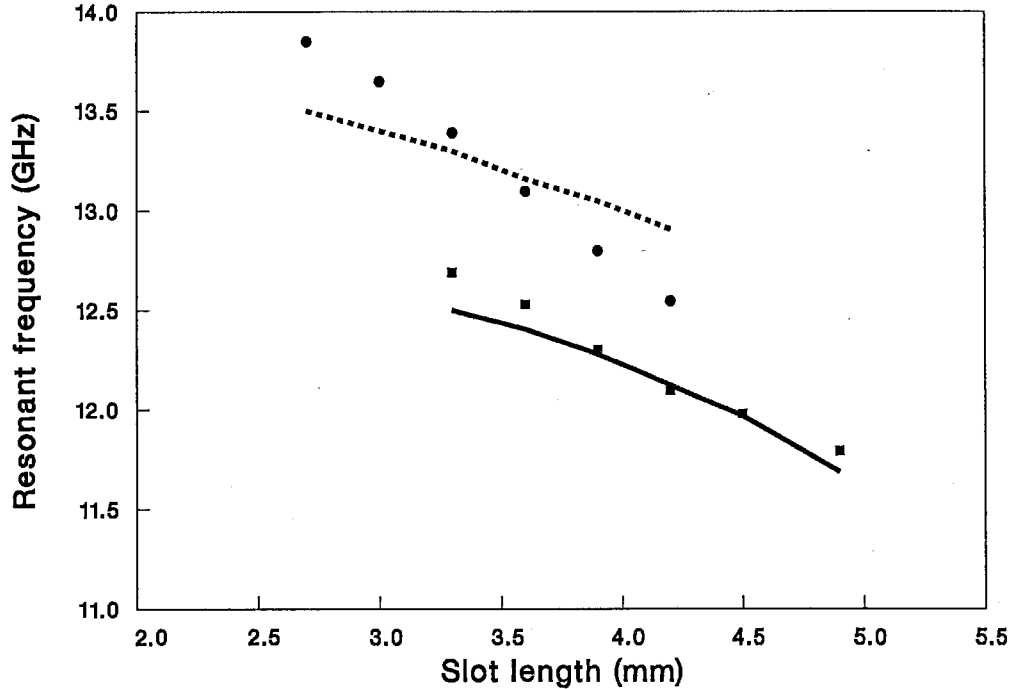


Figure 3.3: Resonant frequency of k_u -band patches as function of slot length

$a = 2.9\text{mm}$, with the other dimensions as given in table 3.2. The substrate thickness is about 6% of the wavelength in the dielectric material at the resonant frequency of the cavity without slot (14.1 GHz). A fixed stub length was used in this case.

Measurements and calculations have been carried out for Ku-band antenna elements, all made of a Poly Phenylene Oxide type substrate (Matsushita R 4726) with relative permittivity $\epsilon_r = 3.4$ and a loss tangent of 0.0065 at 14GHz. Figure 3.4 shows impedance plots of measured and calculated results for a slot coupled patch element in the Ku-band frequency region. The slot length in this case is $L_s = 3.9\text{mm}$, the other data for the geometry are as given in table 3.2. An effective radius $a_{eff} = a + 0.8h$ was chosen to account for the fringing fields at the edge of the cavity.

These examples show, that reasonable accuracy can be achieved in the L-Band frequency range. However, the good coincidence in Ku-band case can only be achieved by introducing an effective patch radius which is different from the one obtained through equation (2.68).

patch	radius	3.13mm	
slot	length	varied	width 0.2mm
substrate 1	height	0.75mm	rel. permittivity 3.4
substrate 2	height	0.6mm	rel. permittivity 3.4
feeding line	width	1.37mm	stublenth 2.93mm

Table 3.2: Dimensions for Ku-band patch element

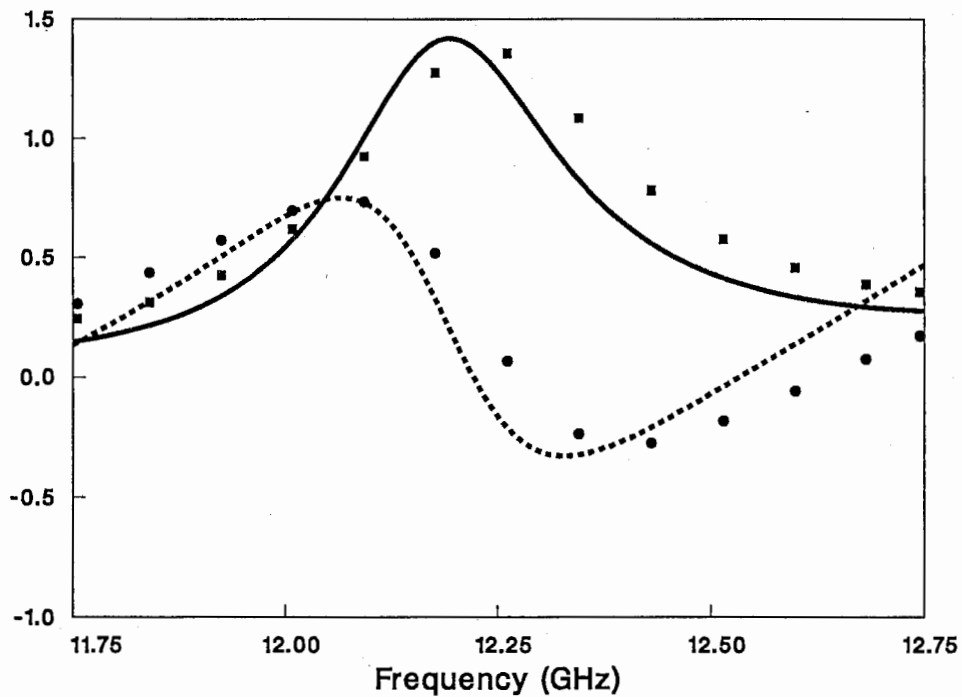


Figure 3.4: Normalized input impedance z_{in} versus frequency (real part of z_{in} : calculated —, measured ■ ■; imaginary part of z_{in} : calculated - - -, measured • •)

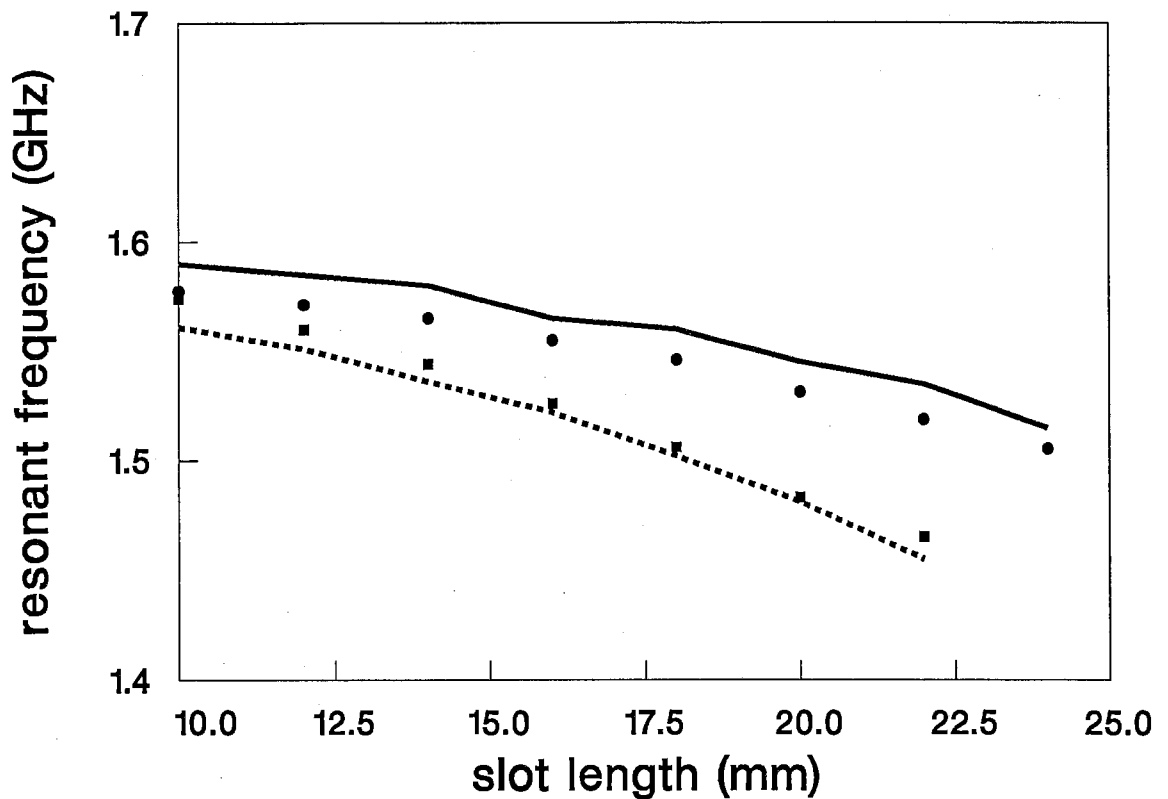


Figure 3.5: Resonant frequency of L-Band patch elements for different slot lengths (patch 1: calculated —, measured • •; patch 2: calculated - - - , measured ■ ■)

3.2 Eigenvector approach

In this section some results are shown, which have been obtained using the eigenvector approach for the calculation of the cavity fields.

Figure 3.5 compares calculated and measured resonant frequencies of two L-band patch elements. Both have been manufactured on a substrate with relative permittivity $\epsilon_r = 2.55$. The other dimensions are given in table 3.3. 50Ω - feed lines have been used in both cases.

A comparison between the calculated and measured real part of the input impedance at the resonant frequency is shown in figure 3.6. The predicted values for resonant frequency and input impedance agree well with experimental results and have a higher accuracy as

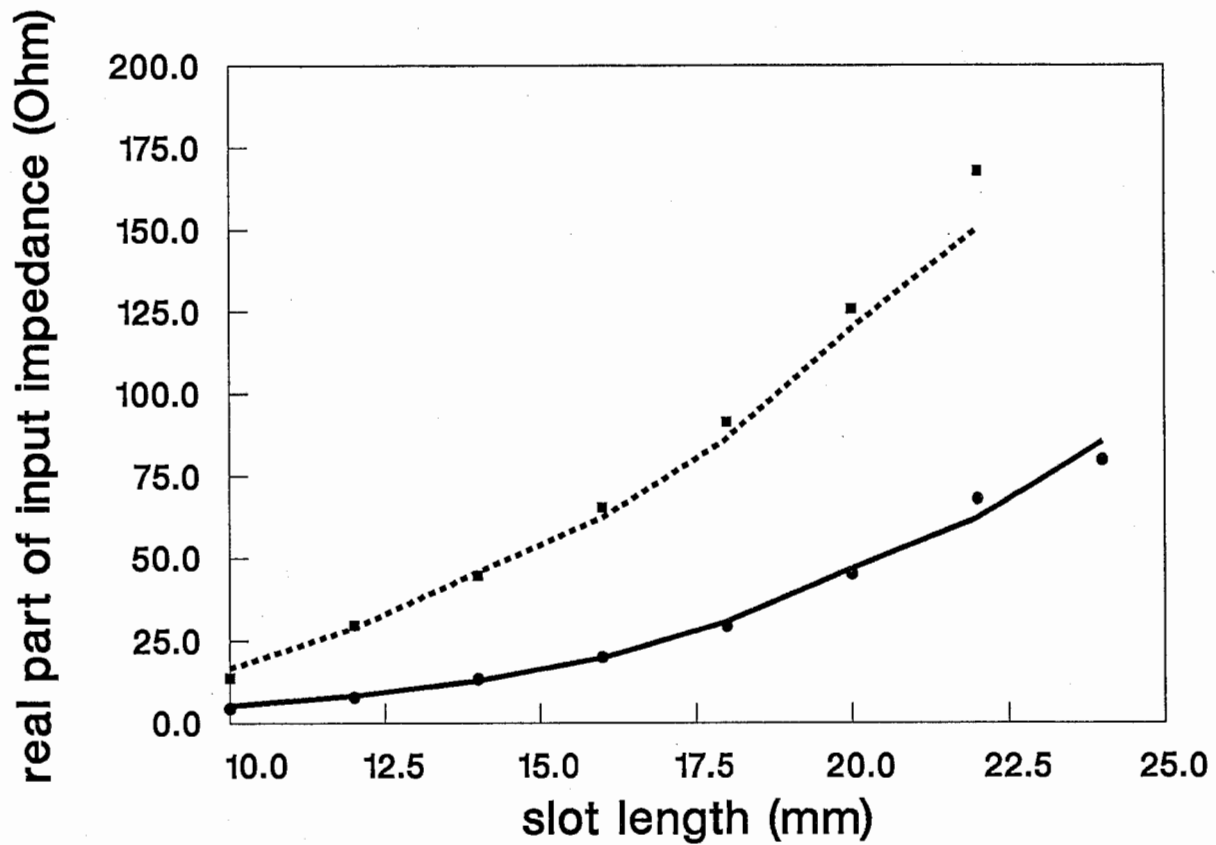


Figure 3.6: Real part of input impedance of L-Band patch elements for different slot lengths at resonant frequency (patch 1: calculated —, measured • •; patch 2: calculated - - - , measured ■ ■)

patch 1	radius 32.63mm	substrate height 3.2mm
patch 2	radius 33.81mm	substrate height 0.8mm
slot	width 1.5mm	length varied
feed substrate	height 1.6mm	rel. permittivity 2.55

Table 3.3: Dimensions of L-band patch elements

patch	radius 3.1mm	
slot	length varied	width 0.2mm
substrate 1	height 0.58mm	rel. permittivity 3.4
substrate 2	height 0.58mm	rel. permittivity 3.4
feeding line	width 1.37mm	stublenth adjusted

Table 3.4: Data for Ku-band patch element

compared to the ones shown in the previous section.

Table 3.4 gives the dimensions of a Ku-band patch element, which has been analysed. The maximum difference between calculated and measured values of the resonant frequency is 3.2% in this example. The comparison between calculated and measured real part of the input impedance at the resonant frequency is shown in figure 3.8. It has to be noted, that the substrate height is 5% of the wavelength in the dielectric at the resonant frequency of the cavity without slot (14.4 GHz).

The next example has the dimensions given in table 3.4, the substrate height was chosen to be $h=0.77\text{mm}$. This is 6.7% of the wavelength in the dielectric at 14.2GHz, which is the resonant frequency of the patch element without slot. Measured and calculated values of the resonant frequency of this patch element are compared in figure 3.9, whereas in figure 3.10 the real part of the input impedance is compared with experimentally obtained values. As expected, there is a degradation in accuracy, which is due to the rather thick patch substrate.

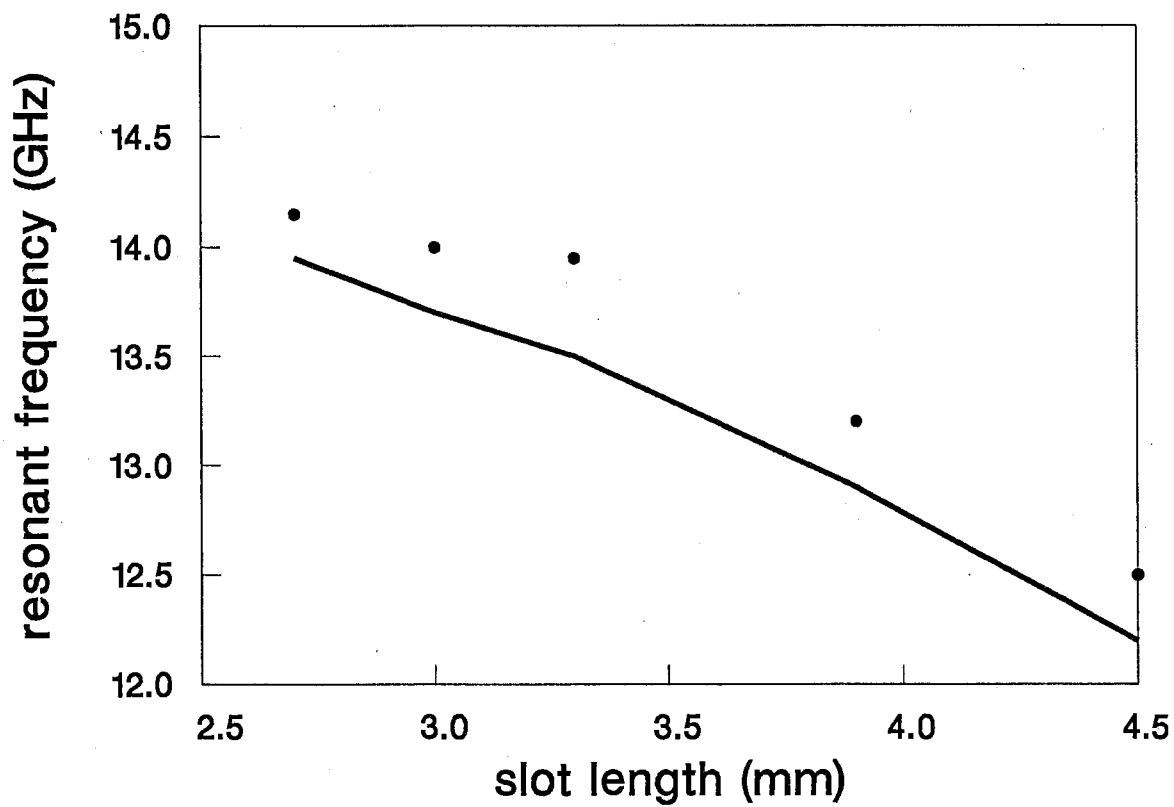


Figure 3.7: Resonant frequency of a Ku-Band patch element for different slot lengths: calculated —, measured • •)

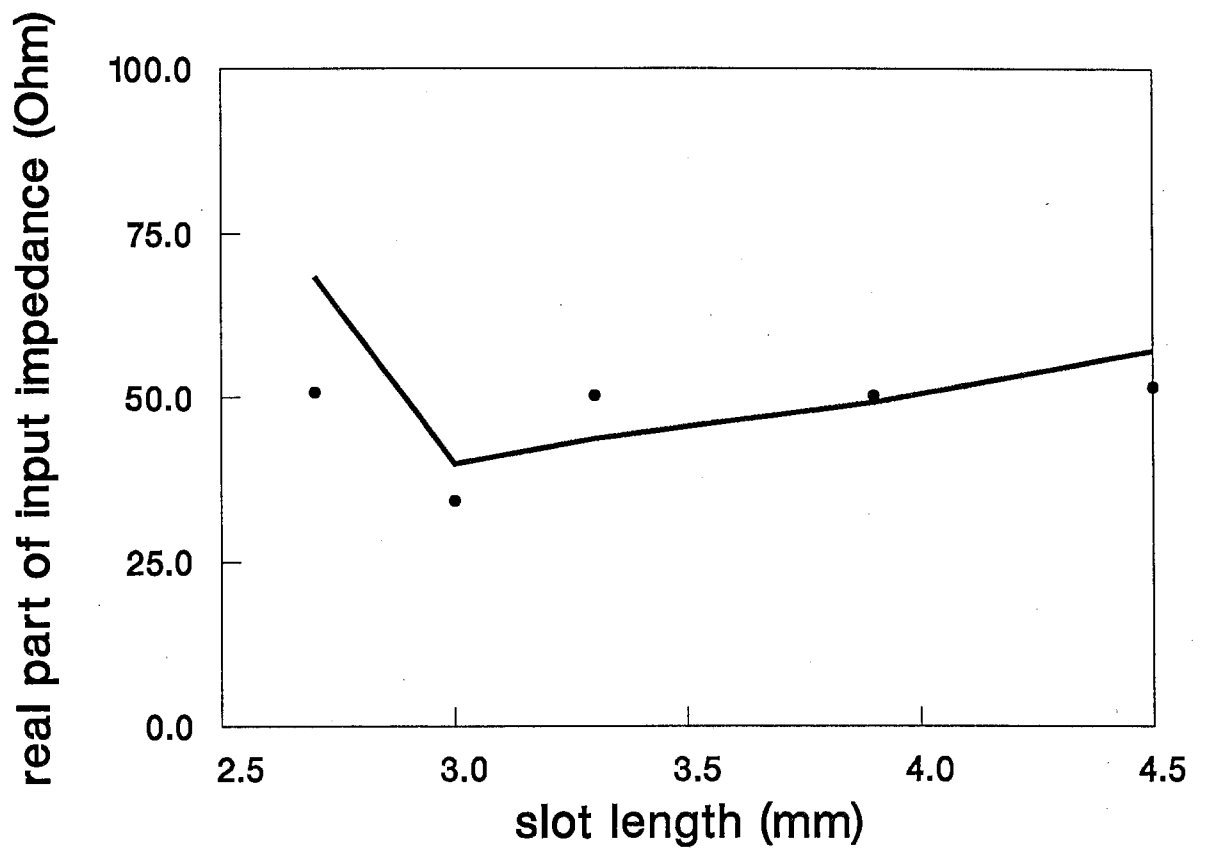


Figure 3.8: Real part of the input impedance of a Ku-Band patch element at the resonant frequency for different slot lengths: calculated —, measured • •)

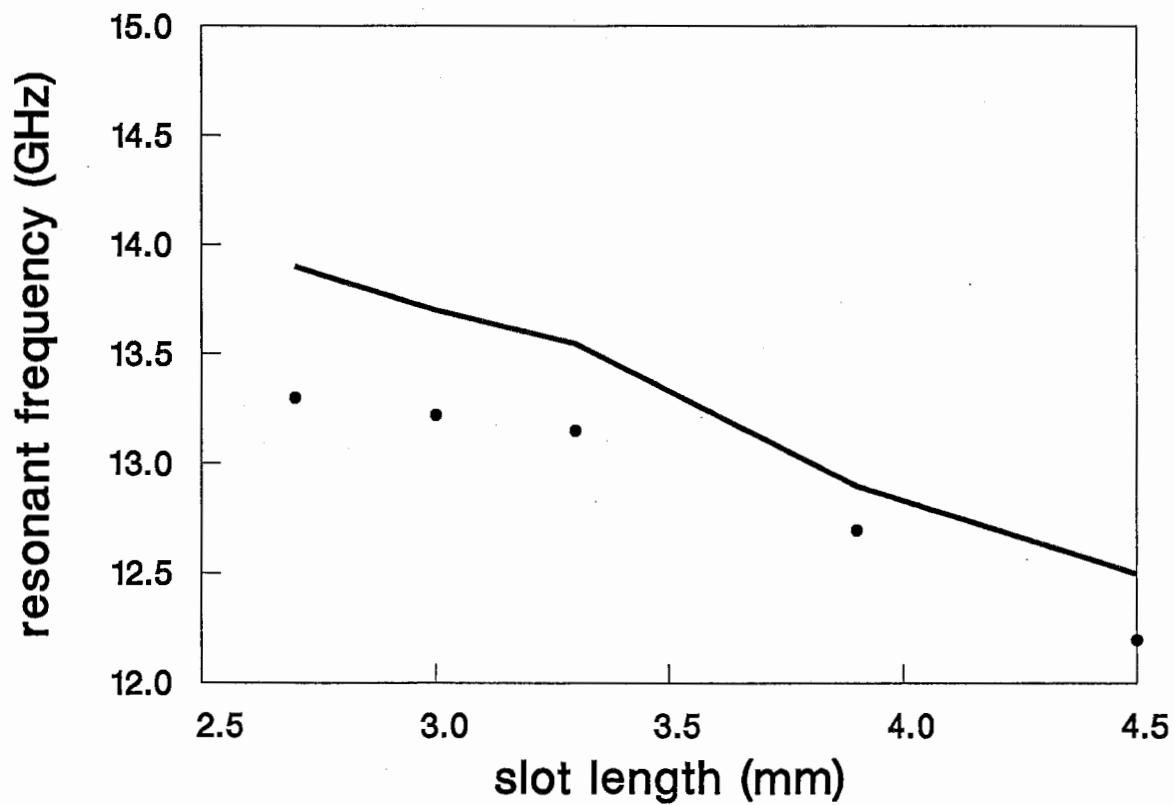


Figure 3.9: Resonant frequency of a Ku-Band patch element for different slot lengths: calculated —, measured • •)

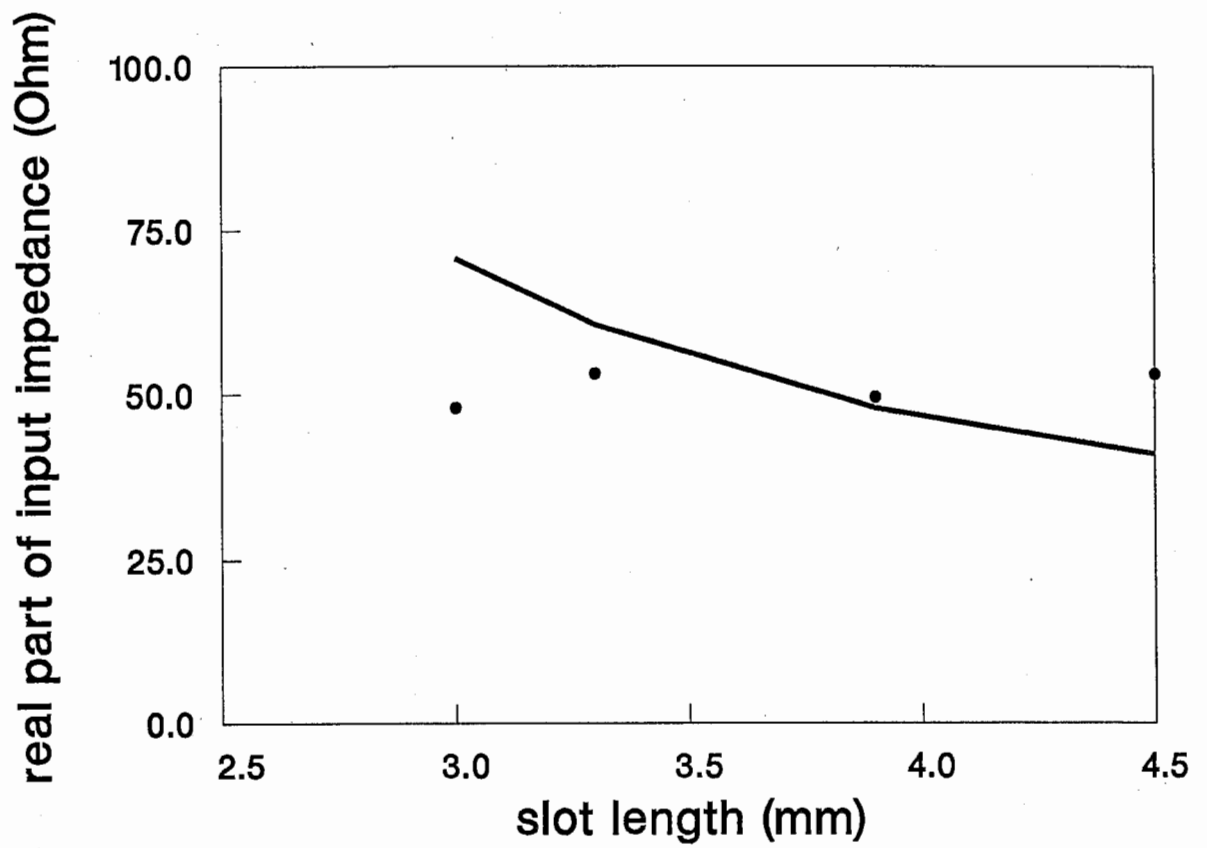


Figure 3.10: Real part of input impedance of a Ku-Band patch element at the resonant frequency for different slot lengths: calculated —, measured • •)

Chapter 4

Summary

A method for calculating the resonance characteristics and the input impedance of slot coupled, circular microstrip patch antennas was presented.

The analysis is based on the idea of conserving the flux of reaction at the coupling aperture, thus making a separation of the complete problem into two parts possible. Each of these two parts can be treated independently.

For the cavity part of the problem, two ways of calculating the fields in a slot loaded cavity have been investigated. One is a Green's function approach in which the Green's function is obtained through an expansion in eigenmodes. In the other method, the fields in the slot loaded cavity are obtained using a splitting in the solenoidal and the irrotational field parts according to Helmholtz' theorem. Each part of the fields is then expanded in its own set of eigenvectors. This seems to provide more accurate results.

The behaviour of the slot in the feeding microstrip line is characterized through the modal voltage discontinuity which is caused by the slot in the ground plane of the microstrip line.

The capabilities of the analysis method have been enhanced by the introduction of parasitic models to account for second order effects, like fringing fields and surface wave effect.

A continuity equation for the flux of reaction is enforced at the coupling aperture after analysing the regions adjacent to the aperture. This is similar to the procedure when the method of moments is used to solve for the coefficients of the aperture field, which is given through an expansion formula in that case. The analysis method explained in this report can therefore be seen as a single term moment method solution. "Single term", because scalars are used to represent the impedances and voltages involved in the analysis. The next step could be a full moment method solution which basically uses the same concept,

but in which the impedances and voltages are represented through matrices. Calculations and measurements agree well in the L-band frequency range. This points to the validity of the proposed approach. The present results for the Ku-band frequency region show a larger relative discrepancy between measured and calculated values. This is partly due to the fact, that the measurements are getting more easily influenced by the shortcomings of the measurement setup. On the other hand, there are still possibilities to enhance the capabilities of the presented approach by treating second order effects more accurately.

At the present stage of this research, it could be demonstrated that the method described is a numerically efficient way to analyse slot coupled, circular patches.

Appendix A

Remarks concerning measurements

A problem, which needs to be investigated carefully, especially at frequencies from Ku-Band on to higher frequencies, is the transition from the microstrip device to the coaxial world outside.

Calibration standards are often not available in the same transmission medium as used for the circuit under test. Then a standard 1-port calibration in the coaxial system is used to calibrate the network analyzer. In this case the influence of the transition has to be kept as small as possible, since it is included in the measurement. Proper care has to be taken in the design of the transitions.

A convenient way to check the quality of the transition, is to use the time domain option of a network analyzer. Fig.(A.1) shows the measured time domain response of an SMA to Microstrip Connector attached to an open microstrip line (length = 30mm, velocity factor = 0.611). It can be seen, that the reflection coefficient of the transition (at $t = 0ns$) is neglectable in this case. The time-domain response shows as well, that the characteristic impedance of the line is slightly smaller than 50Ω .

For a precise measurement the connectors can be characterized in terms of their S-parameters. Methods to derive the S-parameters are for example given in [8], [4]. Once the S-parameters of the transition are determined, they can be used to eliminate the effect of the transitions on the measurements using a desegmentation method [8].

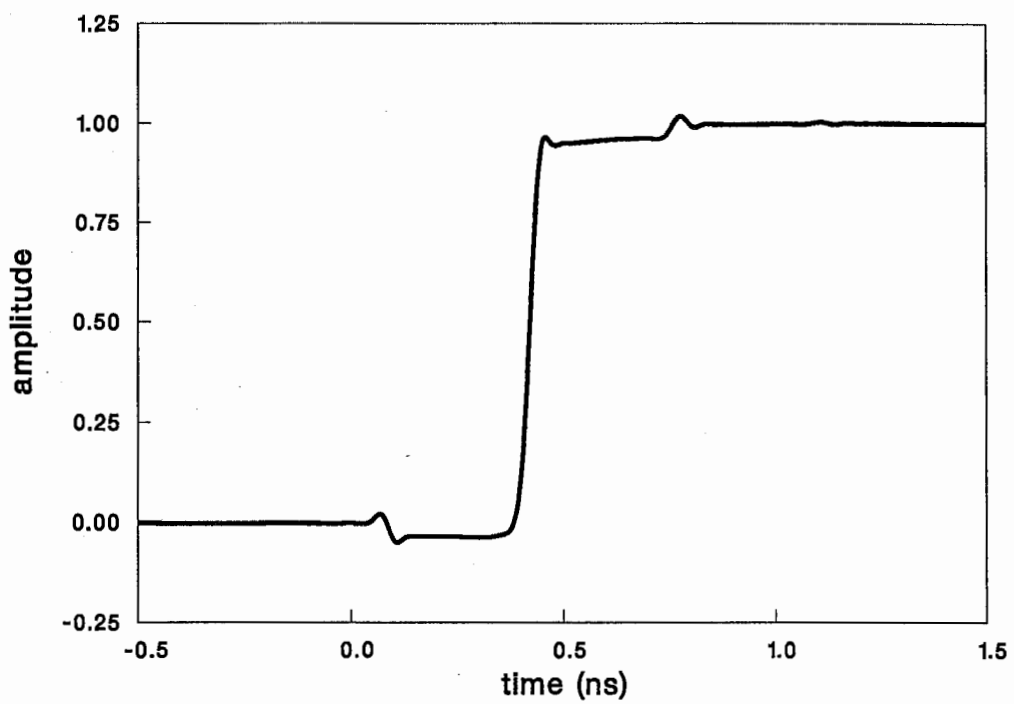


Figure A.1: Time domain response of an SMA-connector attached to an open circuited microstrip line of length $l=30\text{mm}$ and with velocity factor 0.611

Appendix B

Some useful equations

$$\int_0^a [J_m(v)]^2 v dv = \frac{1}{2} v^2 \left[\frac{dJ_m(v)}{dv} \right]^2 + (v^2 - m^2) [J_m(v)]^2 \Big|_0^a \quad (\text{B.1})$$

$$\int_0^a [J_m(k_\rho \rho)]^2 \rho d\rho = \int_0^a [J'_m(k_\rho \rho)]^2 + \frac{m^2}{k_m^2 \rho^2} [J_m(k_\rho \rho)]^2 \rho d\rho \quad (\text{B.2})$$

$$\frac{1}{k_m} \frac{d}{d\rho} J_m(k_\rho \rho) = \frac{-m}{k_m \rho} J_m(k_m \rho) + J_{n-1}(k_m \rho) \quad (\text{B.3})$$

$$= \frac{m}{k_m \rho} J_m(k_m \rho) - J_{n+1}(k_m \rho) \quad (\text{B.4})$$

Bibliography

- [1] M.I. Aksun, S.L. Chuang, and Y.T. Lo. On slot-coupled microstrip antennas and their applications to cp-operation - theory and experiment. *IEEE Transactions on Antenna and Propagation*, Vol. AP-38, pp. 1224 – 1230, 1990.
- [2] I.J. Bahl and P. Bhartia. *Microstrip Antennas*. The Artech House Microwave Library. Artech House, Dedham, Massachusetts, 1980.
- [3] C.A. Balanis. *Advanced Engineering Electromagnetics*. John Wiley & Sons, New York, 1989.
- [4] C. Baumer, U. Bochtler, and F. Landstorfer. Reflexionsarme Übergänge von Koaxialleitung auf Mikrostreifen- und Suspended-Substrate-Leitungen in einfacher Bauform. *Mikrowellen- und HF-Magazin*, Vol. 15, pp. 62 – 66, 1989.
- [5] P. Bhartia, K.V.S. Rao, and R.S. Tomar. *Millimeter-wave microstrip and printed circuit antennas*. The Artech House Antenna Library. Artech House, Boston, 1991.
- [6] W.C. Chew and J.A. Kong. Effects of fringing fields on the capacitance of circular microstrip disk. *IEEE Transactions on Microwave Theory and Techniques*, Vol. 28, No. 2, pp. 98 – 104, 1980.
- [7] R.E. Collin. *Field Theory of Guided Waves*. IEEE Press, Piscataway, 2nd edition, 1991.
- [8] K.C. Gupta, R. Garg, and R. Chadha. *Computer Aided Design of Microwave Circuits*. Artech House, Inc., Norwood, 1981.
- [9] R.F. Harrington. *Time-Harmonic Electromagnetic Fields*. McGraw Hill Book Company, New York, 1987.
- [10] M. Himdi and J.P. Daniel. Characteristics of sandwich-slotlines in front of a parallel metallic strip. *Electronics Letters*, Vol. 27, No. 5, pp. 455 – 457, 1991.

- [11] M. Himdi, J.P. Daniel, and C. Terret. Analysis of aperture-coupled microstrip-antenna using cavity method. *Electronics Letters*, Vol. 25, No. 6, pp. 391 – 392, 1989.
- [12] R.K. Hoffmann. *Integrierte Mikrowellenschaltungen*. Springer Verlag, Berlin, 1983.
- [13] T. Itoh, editor. *Numerical Techniques for Microwave and Millimeter-Wave Structures*. John Wiley & Sons, New York, 1989.
- [14] A. Ittipiboon, R. Oostlander, and Y. Antar. Modal expansion method of analysis for slot-coupled microstrip antenna. *Electronics Letters*, Vol. 25, No. 20, pp. 1338 – 1340, 1989.
- [15] D. Jackson and N. Alexopoulos. Simple formulas for the input impedance, bandwidth, and radiation efficiency of a rectangular patch. *IEEE Int. Symp. Digest Antennas and Propagation*, pp. 1130 – 1133, 1989.
- [16] J.R. James, P.S. Hall, and C. Wood. *Microstrip Antenna Theory and Design*. IEE Electromagnetic Waves Series 12. Peter Peregrinus Ltd., London, 1981.
- [17] J.R. James and A. Henderson. High-frequency behaviour of microstrip open-circuit terminations. *IEE Journal of Microwaves, Optics and Acoustics*, Vol. 3, pp. 205 – 218, 1979.
- [18] Y.T. Lo and S.W. Lee. *Antenna Handbook*. van Nostrand Reinhold Company, New York, 1988.
- [19] P. Perlmutter, S. Shtrikman, and D. Treves. Electric current model for the analysis of microstrip antennas with application to rectangular elements. *IEEE Transactions on Antenna and Propagation*, Vol. 33, pp. 301 – 311, 1985.
- [20] D.M. Pozar. Microstrip antenna aperture coupled to a microstripline. *Electronics Letters*, Vol. 21, No. 2, pp. 49 – 50, 1985.
- [21] D.M. Pozar. A reciprocity method of analysis for printed slot and slot-coupled microstrip antennas. *IEEE Transactions on Antenna and Propagation*, Vol. AP-34, pp. 1439 – 1446, 1986.
- [22] F.W. Richards, Y.T. Lo, and D.D. Harrison. An improved theory for microstrip antennas and applications. *IEEE Transactions on Antenna and Propagation*, Vol. AP-29, pp. 38 – 46, 1981.

- [23] T.K. Sarkar and E. Arvas. An integral equation approach to the analysis of finite microstrip antennas: Volume/surface formulation. *IEEE Transactions on Antenna and Propagation*, Vol. 38, No. 3, pp. 305 – 312, March 1990.
- [24] L.C. Shen, S.A. Long, M.R. Allarding, and M.D. Walton. Resonant frequency of a circular disk printed circuit antenna. *IEEE Transactions on Antenna and Propagation*, Vol. AP-25, pp. 595– 596, 1977.
- [25] Shigihara and Iwasaki. Slot coupled microstrip antennas. Technical Report TR-O-0035, ATR Optical and Radio Communications Research Laboratories, Kyoto, Japan, 1989.
- [26] J.C. Slater. *Microwave Electronics*. Van Nostrand Company, Inc., Princeton, 1950.
- [27] P.L. Sullivan and D.H. Schaubert. Analysis of an aperture coupled microstrip antenna. *IEEE Transactions on Antenna and Propagation*, Vol. AP-34, pp. 977 – 984, 1986.
- [28] A.K. Verma and Z. Rostamy. Modified Wolff model for determination of resonance frequency of dielectric covered circular microstrip patch antenna. *Electronics Letters*, Vol. 27, pp. 2234 – 2236, 1991.
- [29] C. Wood. Analysis of microstrip circular patch antennas. *Proceedings of the IEE*, Vol. 128 H, pp. 69 – 76, 1981.